Estimating Subsurface Topography from Surface-to-Borehole Seismic Studies at the Rye Patch Geothermal Reservoir

Roland Gritto[1,*], Thomas M. Daley[1] and Ernest L. Majer [1]

Short title: SEISMIC MAPPING AT RYE PATCH

Abstract.

A 3-D surface seismic reflection survey, covering an area of over 7.7 km^2, was conducted at the Rye Patch geothermal reservoir (Nevada) to explore the structural features that may control geothermal production in the area. In addition to the surface sources and receivers, a high-temperature three-component seismometer was deployed in a borehole at a depth of 1190 m within the basement below the reservoir, which recorded the waves generated by all surface sources. The objective of this study was to determine the subsurface structure of the reservoir based on this surface-to-borehole dataset. A total of 1959 first-arrival travel times were determined out of 2134 possible traces. Two-dimensional ray tracing was performed to simulate wave propagation from the surface sources to the receiver at depth. The ray tracing was based on a 2-D laterally homogeneous velocity model derived from results of a vertical-seismic-profile (VSP) experiment recorded in the same well. It is assumed that differences in travel time between the observed and modeled data are caused by structural deviations from a homogeneously layered model as estimated by the VSP profile, and thus are mapped into topographic changes at depth. The results indicate the presence of two dominant geologic features. The first confirms the regional trend of the geologic units in the Basin and Range province with a north-south strike and dip to the west, as expected for this area to the west of the Humbold Trust Range. The second is a local disturbance of this regional pattern in form of an elevation of the interface between the carbonate basement and the overlying sedimentary sequence, striking east-west cross-cutting through the westward dipping units along the western boundary of the survey area. The geometry of the structure is corroborated by results from a seismic-reflection survey, and by results of a gravity survey conducted in the area above the reservoir.

Introduction

Geothermal reservoirs are considered difficult seismic targets because of hydrothermal alteration and structural heterogeneity (Blackwell, 1985; Sorey, 1985). In the 1960s and 1970s, seismic experiments were started to determine the subsurface structure of Long Valley Caldera, California, and to more tightly constrain the geometry of the caldera floor (Pakiser et al., 1960; *Hill*, 1976). The results showed several sequences of shallow and deep reflectors interrupted by faulting, although no conclusive evidence for the presence of a hypothesized magma chamber was reported. These early studies revealed the problems associated with the application of seismic methods to geothermal areas. In the past 30 years, technological advances in seismic exploration have increased the impact of seismic surveys on hydro-carbon prospecting. Although 2-D and 3-D seismic methods have proven to be an integral part of modern oil and gas exploration efforts, the heterogeneous nature of geothermal reservoirs makes all seismic imaging more difficult (Black et al., 1991; Hill et al., 1976). It is only beginning to emerge how well exploration methods used in the petroleum industry can be transferred to the geothermal industry.

In recent years, seismic surface and borehole experiments were conducted at the Rye Patch geothermal reservoir, Nevada, to determine the geologic structure of the (hypothesized) fault-controlled reservoir. The Rye Patch geothermal reservoir is located in Pershing County, Nevada, along the east side of Interstate 80, about 200 km northeast of Reno. Commercial development of the Rye Patch geothermal project started in the late 1980s and resulted in the construction of a 12 MW powerplant and eight geothermal wells, of which seven were either too cold or non-productive. In the successful well, however, significant production at reservoir temperatures in access of 200 °C was encountered. The eight boreholes were drilled within an area of less than one square mile, which indicated that distribution of reservoir fluids is most likely controlled by fractures and faulting with limited areal extent. In 1997, The Industrial Corporation

(TIC), as the owner of the project, and Transpacific Geothermal Inc. (TGI), cooperated with the Lawrence Berkeley National Laboratory (LBNL) to evaluate and apply modern seismic-imaging methods for geothermal-reservoir definition under the U.S. Department of Energy's (DOE) Geothermal Program. As part of this effort, a vertical seismic profile (VSP) was acquired in 1997 to determine the seismic reflectivity of the reservoir horizons and to obtain reservoir velocity information. Because the results of the initial VSP profile indicated apparent reflections at depth (*Feighner et al.*, 1998), the participants in the project decided to proceed with a 3-D seismic-reflection survey, which was acquired in 1998.

As part of the seismic surface survey, an additional surface-to-borehole experiment was conducted, during which a three-component high-temperature geophone was installed in the original VSP well at a depth of 1190 m. This geophone recorded all seismic waves generated by the surface sources, creating a second dataset in addition to the seismic-reflection data. The locations of the 3-D surface survey and of borehole 46-28 containing the geophone at depth are indicated in Figure 1 (modified after *GeothermEx*, 1997). They coincide with the Rye Patch temperature anomaly, which is bounded by the Humbold City Thrust in the East and the Rye Patch reservoir in the West. Results of the 3-D seismic survey were presented by *Feighner et al.* (1999) and revealed possible faulting at depth based on surface seismic-reflection studies and surface-to-surface tomographic-travel-time investigations. In the current study, we present the results of the surface-to-borehole dataset, which was recorded with minimal extra effort during the acquisition of the surface-reflection survey, and show that it can provide additional valuable information, which confirms the results of previous studies, about the reservoir structure at depth.

Data Acquisition and Processing

The Rye Patch Geothermal survey covered an area of approximately three square miles and was designed with 12 north-south receiver lines and 25 east-west source lines. The source interval was 100 feet, whereas the source line spacing was 400 feet. Four Litton 311 vibrators were used in a squared array, with the source flag at its center. The source signal was a sweep with frequency bandwidth between 8 Hz and 60 Hz. A detailed description of the data collection can be found in the contractor's report (*SECO*, 1998).

A high-temperature, wall-locking, three-component geophone was installed in well 46-28 at a depth of 1190 m. The borehole geophone recorded all shots throughout the survey area, amounting to a total of 2134 traces. The location of all sources as well as the boreholes are shown in Figure 2. The gaps in coverage are caused by Interstate 80 and railroad tracks, which cross the survey area in a north-south direction.

The data quality is good, with a central frequency content of about 25 Hz for the first arriving waves. Figure 3 shows a representative receiver gather of a source line about 1200 m north of well 46-28. It is evident, as a first-order effect, that the moveout of the first arriving waves vary with distance to the well. Additionally, local and smaller variations in arrival time can be seen between source positions 10048 and 10063. These local variations in travel time will be mapped into topographic changes of the reservoir horizons at depth.

A total of 1959 first-arrival travel times were determined out of 2134 possible traces. Most of the picks are reliable because the well-sampled spatial moveout across the source lines facilitated the picking. However, in addition to the long source lines, "make-up lines" with shorter distances and a maximum number of nine sources per line were set up in between the original lines. The first-arrival picking was less reliable for these shorter lines.

Ray Tracing

In 1997, a VSP was recorded at the Rye Patch Geothermal field in well 46-28 (*Feighner et al.*, 1998). The resulting P-wave velocity profile between the depth of 120 m and 1265 m represents the best estimate for the distribution of velocities in the subsurface around the well, and is the only *in situ* velocity measurement available. Based on these results, we derived a velocity function that represents a smoothed average of the VSP velocity profile. The function and its geologic interpretation are shown in Figure 4. The prominent features of this velocity function are the high-velocity layer of 3500 m/s between 210 m and 240 m depth, followed by a velocity inversion to approximately 2750 m/s down to a depth of 700 m. This upper interval represents the Tertiary sequence of sedimentary and volcanic rocks. Below this sequence lie the carbonates of the Triassic basement rocks, indicated by a velocity increase to about 6100 m/s. The productive zone of the reservoir is confined to a clastic layer of 60 m thickness at a depth of about 880 m within the carbonates. However, this thin layer is not resolved in the velocity function shown in Figure 4.

This velocity profile is subsequently extended to a 2-D velocity model with homogeneous layers extending throughout the survey area. Based on this velocity model, 2-D ray tracing is performed to simulate wave propagation from surface sources to the receiver at depth. Figure 5 shows representative results of the ray tracing. The velocity model is a 2-D representation of the function in Figure 4. Sources are denoted by stars, while the receiver is indicated by an inverted triangle at 1190 m depth. Figure 5a represents the rays for a source line that runs in an east-west direction across well 46-28, while Figure 5b shows a line running across the well in a north-south direction. The gaps in source coverage indicate the railroad tracks, Interstate 80, and an area in the vicinity of the well where no sources were fired. The top of the velocity model is chosen to be equal to the elevation of the highest source position of the survey, which causes the sources in Figure 5 to appear to be located below the surface.

The 2-D raytracing produces a total of 2134 rays, connecting the sources to the receiver at depth, and their associated travel times. None of the 2134 rays crosses the paths of other rays, which prevents the application of a tomographic inversion approach. Therefore, it is not possible to estimate lateral velocity variations within the layers. However, under the assumption that the original geologic sequences were deposited in layers, and that subsequent disturbances of the stratigraphy were caused by faults, the topographic structure of the reservoir can be mapped by comparing observed to numerically calculated travel times. In the current example, the velocity structure estimated from the VSP experiment is used as a reference model, and travel times are calculated for all surface sources. The observed and calculated travel times are compared for each source-receiver combination, and differences attributed to changes in elevation of the subsurface horizons. This method will be explained in the next section.

Although most geothermal reservoirs exhibit localized heterogeneity caused by areas of hydrothermal alteration as well as volcanic deposition (i.e., basaltic lenses), these areas are confined to relatively small volumes (in the case of lenses) or thin sheets (in the case of hydrothermal alteration along fluid pathways). The main reason for geothermal reservoir heterogeneity is faulting, which juxtaposes large volumes of sedimentary and volcanic layers of different origin. This type of heterogeneity has the largest effect on travel times of seismic waves propagating through the reservoir. Therefore, it is reasonable to assume, to first order, that the deviations between observed and calculated travel times based on a horizontally layered reference model are caused by faulting, and that the travel-time differences can be used to map large structural features throughout the reservoir.

Mapping Travel-Time Deviations to Elevation Changes at Depth

Methodology

Mapping travel-time deviations to elevation changes is a technique that has been used in seismic refraction studies in the past, and is also referred to as "seismic detailing (Dix, 1952), time-term method, or delay-time method (Telford et al., 1990; Nettleton, 1940). The method is an approximation that can be applied to environments where a low-velocity layer is located above a high-velocity layer. Under the assumption that the ray path from source to receiver is known, any difference between the calculated and observed travel times is converted into a distance using the velocity model and applied as a deviation in the boundary between the two layers. The same principle is applied in the current approach assuming that the top layer is represented by the 700 m thick sedimentary and volcanic Tertiary sequence, which can be approximated by an average velocity of 2750 m/s; whereas the Triassic carbonates of the basement are represented by a halfspace with a velocity of 6100 m/s (refer to Figure 4).

Figure 6 represents a schematic model of a low-velocity layer overlying a high velocity basement ($v_1 < v_2$). A geophone is positioned in a borehole at a total depth $z = h_1 + h_2$, while a source is located at the surface at a distance x from the well-head. The total travel time t_m from source to receiver can be expressed by ray theory as

$$t_m = \frac{x}{c} + \frac{h_1 cos\alpha_1}{v_1} + \frac{h_2 cos\alpha_2}{v_2}, \tag{1}$$

where $\frac{1}{c}$ is the ray-parameter, which is constant along the seismic ray from source to receiver and

$$\frac{sin\alpha_1}{v_1} = \frac{sin\alpha_2}{v_2} = \frac{1}{c}. \tag{2}$$

If the boundary between the layer and the basement is perturbed by a difference in

elevation of δh (refer to Figure 6), the observed travel time becomes

$$t_o = \frac{x}{c} + \frac{(h_1 + \delta h)cos\alpha_1}{v_1} + \frac{(h_2 - \delta h)cos\alpha_2}{v_2}, \tag{3}$$

where Fermat's principle has been invoked by assuming that α_1 and α_2 do not change. Thus, the difference in travel time between the unperturbed and perturbed case is

$$\delta t = t_m - t_o = \delta h(\frac{cos\alpha_2}{v_2} - \frac{cos\alpha_1}{v_1}), \tag{4}$$

and the elevation difference becomes

$$\delta h = \frac{\delta t}{(\frac{cos\alpha_2}{v_2} - \frac{cos\alpha_1}{v_1})}. \tag{5}$$

Since Fermat's principle states that the arrival time is stationary with respect to the perturbation of the ray path around the original one, it can be calculated along the unperturbed ray instead of the perturbed one (*Aki and Richards*, 1980). This is the basis for the current mapping approach, where the elevation difference δh is projected along the unperturbed ray in the layered velocity model.

Although the identification and mapping of faults at Rye Patch reservoir has proved difficult, several geophysical surveys, including surface magnetic, gravity, self-potential, and seismic reflection in conjunction with geological observations, suggest the existence of at least one east-west striking fault (*GeothermEx*, 1997; *Teplow*, 1999). The depth extension of the fault has been estimated to reach from a minimum depth of 1500 m in the Triassic carbonate basement upwards into the shallow parts of the Tertiary sediments, without producing evidence at the surface. This model is the basis for the current interpretation, where it is assumed that the fault starting in the carbonates cuts upwards through the thin clastic reservoir layer at 880 m depth, as well as through the carbonate-sediment interface at 700 m depth. This assumption requires a minimum depth extension of 180 m for the fault, which is well within the range estimated from geophysical and geological data at Rye Patch.

Once the elevation changes are computed for the two-layered model mentioned above, they need to be migrated along the rays to be mapped at the locations where the rays cross the boundary between the sedimentary layer and the basement. The results of the migration are presented in Figure 7. The locations of the surface sources are indicated by the grey circles, while the locations of the rays refracting through the sedimentary-basement interface are given by the black dots, which indicates the area of the interface that can be mapped by the present dataset.

Seismic Mapping and Source Elevation Statics

Equation (5) was used to map travel-time changes to changes in elevation at depth. Positive deviations denote source positions from which the actual waves travel faster to the receiver than in the ray tracing simulations. The assumed interpretation in this case is that the high velocity basement is uplifted relative to the homogeneously layered velocity model used in the simulations. Similarly, negative deviations denote slower wave propagation than assumed in the simulations, indicating a thicker low-velocity layer on top of the basement (i.e., the basement is shifted downwards, refer to Figure 5).

The results of mapping the travel-time change δt to changes in topography are given in Figure 8. The figure shows a surface plot generated from 1959 data points representing the total number of first-arrival times determined from the data. Under the assumption that the above interpretation is correct Figure 8 would depict the topographic deviations in the interface between the carbonates and sediments at 700 m depth. To first order, this interface reveals higher values in the east, which gradually decrease towards the western boundary of the survey area. However, it is evident that the trend of this interface also mimics the dip in elevation of the surface sources throughout the survey area, as shown by the 3-D map in Figure 9. The source elevation decreases towards the west following the dip of the surface from the Humboldt City Thrust in the east to the Rye Patch Reservoir in the West (refer to Figure 1).

The problem that can occur using correct source locations with large elevation changes while applying a constant velocity model for the near surface layer is that geologic processes often compensate for the shortcomings of this model. While the travel distance from sources at high elevation to the receiver at depth is longer, these source sites are usually exposed to stronger erosion, which removes the low velocity sedimentary layers, and thus hard rock with higher velocities may be exposed to compensate for the longer travel distance. If, during the simulations, sources are placed at the correct elevations in conjunction with the use of a low-velocity surface layer, the travel times of the simulations may become too long relative to the observed travel times and, as a consequence, larger travel time deviations are observed. The reverse effect may take place for lower elevations, where thicker sedimentary fill can lower the values of the velocity below those assumed in the model.

Thus, a second simulation is performed to verify that the trend of the interface in Figure 8 is not an artifact caused by the distribution of source locations during the survey. During this test all sources are located at a fixed level equal to the elevation at the well head of borehole 46-28. If the structure in Figure 8 is caused by static problems with the source locations, it would disappear or change after the simulations with a flat source-horizon. However, a similar structure is produced as a result of this test, as shown in Figure 10. Although the overall elevation changes decrease slightly, relative to the results in Figure 8, the general feature of an elevation high in the central eastern region of the survey area decreasing towards the west is still evident. Therefore, it is assumed that static time shifts associated with local inhomogeneities in the vicinity of the surface sources represent a secondary effect that can be neglected for the purpose of this study. Contrary to the eastern region of the survey area, the western half reveals a pronounced trend to negative elevation changes. These deviations are only partially reduced by the introduction of a flat source horizon in Figure 10. This feature may indicate a rapid deepening of the basement to the west created by north-south trending

normal faults, which constitute the dominant structural mechanism in the Basin and Range province.

A closer look at Figure 8 reveals local topographic changes superimposed on the gradual westward dip of the interface. The central eastern region of the survey area, east of well 72-28, is dominated by an increase in elevation that is gradually decreasing towards north and south. Similarly, in the central western part of the area, the gradual dip of the interface is interrupted by an increase in elevation. It seems that a structural feature striking east-west lifts the basement interface in the eastern and even in the western region although the total topography change remains negative in the western part of the survey area. Thus it appears that the analysis revealed two main features within the Rye Patch reservoir. The first is the expected dip of the geologic units towards the West associated with normal faulting on a regional scale, while the second is a local unconformity, which seems to be supported by east-west faulting perpendicular to the regional trend.

Error Analysis

The maximum estimated topography change in Figure 8 is 498 m, while the average deviation is 122 m. These estimates may appear high compared to the depth of the interface between the upper sedimentary layer and the carbonate basement, which is modeled at a depth of 700 m. To check these apparently high estimates, we perform a numerical test to determine whether these magnitudes of elevation changes could be recovered with the current method. A representative source line is chosen, which covers the lateral extent of the farthest source positions in the field experiment, with the idea that ray paths to large offsets will reveal the strongest discrepancy between the two chosen velocity models. The first reference model is the same as above, with a 700 m thick low-velocity layer (2750 m/s) over a high-velocity basement (6100 m/s). In a second model, the interface is uplifted by 500 m to a depth of 200 m, representing the

extreme elevation changes encountered in the current results. Ray tracing is performed for both models, and the travel-time differences mapped into elevation changes. The comparison between estimated and modeled elevation yields a standard deviation of 1.9% (29.6 m). In a third model, the interface is lifted by 122 m, the average deviation estimated from the field data, and travel-time differences to the reference model are mapped to elevation changes again. The results produce a standard deviation of 1.1% (1.3 m). These values can be regarded as uncertainties in the mapping procedure and are well within the range of accuracy intended for the current analysis. The actual elevation changes of the basement horizon are likely to be smaller than the ones shown in the present mapping, since all deviations from the assumed horizontally layered velocity model are mapped into elevation changes. Additionally, the velocity model may not be a good representation at great distances from the borehole, and it is feasible that a deviation in travel time is caused by a local velocity unconformity rather than a change in a boundary of the layered velocity model. However, it is not possible to estimate those local velocity changes with the present data, because this would require a solution to a complex inversion problem, for which data coverage with numerous crossing rays is needed. The current dataset, however, does not contain any crossing rays in the subsurface. Thus, the estimated changes in elevation should be considered as representations of the upper bounds for the actual values. With these considerations in mind, the structure of the interface will be investigated more closely.

Interpretation and Comparison to Previous Studies

A mapview of the basement horizon elevation is provided in Figure 11. The three boreholes 46-28, 44-28, and 42-28 are shown for reference. It can be seen that the 0 m elevation contour line runs through well 46-28, which is a confirmation that the smooth version of the velocity model shown in Figure 4 is a good representation of the actual velocities in the vicinity of well 46-28. The map shows the contours of the elevated

structure extending from east to west, elevating the basement interface in the East while cutting through the steep descent on the western flank. The north-south extent of this rise reaches roughly from state coordinate 2107000 (north of well 42-28) to 2100000 (south of well 46-28).

In addition to the source locations shown in Figure 2, four far-offset source locations were selected during the 3-D seismic survey in 1998, to obtain far-offset refracted first-arrival data that could be used to determine the deeper velocity structure. The far offset shots were recorded by 10 receiver lines in the center of the survey. Data quality varied significantly for each of the four shots, indicating regional heterogeneity. The qualitatively best datasets resulted from shot number 2, located 7.4 km NW of the VSP well 46-28, and shot number 4, located 5.2 km SSE of the well.

Figure 12 shows the data for far-offset shot number 2 recorded by a receiver line in the western half of the survey area. The northern receivers recorded sharp first arrivals, but the signal is abruptly attenuated for the receivers in the central and southern part of the survey area. This pattern was consistent for the other receiver lines. The two grey areas in Figure 11 represent the receiver locations where the first-arrival energy was clearly visible. The northern polygon represents the arrivals of the data recorded from shot number 2 to the northwest, while the southern polygon represents those of shot number 4 to the south. It is evident from the figure that the central area had weak or non-existing first arrival energy. A possible interpretation is the existence of faults where seismic energy is scattered and attenuated. Since the boundaries of the polygons match the outline of the elevated structure quite well, it could be concluded that faults, bounding the elevated structure to the north and south, attenuated the seismic waves from the far offset shots.

The location of a possible fault was interpreted by *Teplow* (1999) based on 3-D seismic reflection data. The intersection of the fault with the clastic reservoir unit had a strike of N 76° W and a dip of 73° NNE. The intersection of this fault with

the sedimentary-carbonate interface is indicated by the dark-grey line in Figure 11 immediately south of well 44-28. In projecting the fault upward onto this interface, a constant strike and dip is assumed. The interpretation of the east-west extension of the fault was limited because of the poor continuity of reflected seismic energy in the east-west direction (*Teplow*, 1999). It can be seen that the strike-line of the fault coincides with the boundary of the southern zone that marks the transition from strong to weak first arrival energy, and is co-located with the southern flank of the elevated structure indicated by the contour lines. Thus a possible interpretation is that the elevated structure is a manifestation of the postulated fault.

The study by *Teplow* (1999) also included a gravity survey of the Rye Patch geothermal field. The survey consisted of 334 stations along 19.8 km of profile lines and was located in the central region of the seismic survey. Figure 13 shows the Bouguer gravity residual of the central Rye Patch reservoir. The contour lines show a dipping structure in the western region of the survey, indicating a deepening of the basement to the west that was also evident in the seismic data above. The central region of the survey is dominated by a gravity high located around the boreholes. Possible explanations for this gravity high could be a densification of the reservoir or basement rocks resulting from hydrothermal mineralization, or the uplift of basement rocks with high density, relative to the overlying sediments with lower density. The thick black line in Figure 13 represents the 0 m-elevation contour of the basement interface as estimated from the seismic data in Figure 11. The comparison to the gravity residual shows a general conformity in shape, although the extent of the seismic contour line reaches farther to the west. The combination of seismic and gravity data could possibly suggest the presence of an elevated basement structure, while the process of localized densification may not be applicable to explain the seismic data. Although hydrothermal mineralization can increase seismic velocities relative to the surrounding host rock, it usually occurs along leaks from the production zone of the reservoir, preferentially

along faults or other weak structures, producing one- or two-dimensional alterations. However, the volume of faster material needed to match the observed seismic travel time differences is considerably larger than that produced by hydrothermal alterations (see Figure 8).

A feature similar to the elevated structure described above was reported by *Feighner et al.* (1999), and is shown in Figure 14. The figure shows tomographic velocity estimates from two receiver lines along the eastern boundary of the survey area. Although the depth penetration for the tomographic study is limited as the turning rays propagate from surface sources to surface receivers, the ray coverage is good down to 500 m depth. The two vertical lines in Figure 14 indicate the location of the 200 m contour line representing the center of the elevated structure at the eastern boundary of the survey in Figure 11. The tomographic estimates reveal an elevated structure of faster material in the center of the survey area. It should be noted that the elevated velocity contours at the margins of the images in Figure 14 are an artifact of the ray geometry and do not represent actual subsurface structure. However, both depth sections indicate a broad range of elevated high-velocity material in the central and south-central section of the survey area, which is in agreement with the results presented in Figures 8 and 11. Thus it appears that the elevated high-velocity structure defining the interface between basement and overlying sediments extends upward without breaking the surface, because the velocity contours in Figure 14 seem to flatten out in the upper 50 m.

Conclusions

The 3-D seismic experiment conducted at Rye Patch geothermal field provided a series of datasets and methods to image and interpret the subsurface structure of the reservoir (surface reflection seismic, surface-to-surface tomography, and surface-to-borehole seismic mapping). The addition of a depth geophone to record surface-generated seismic waves during the 3-D reflection survey provided an independent dataset at

low cost and minimum technical and labor requirements. Because most geothermal areas provide access to open boreholes during the developing stages of the reservoir, it is recommended that a VSP survey is conducted first, to obtain information about the velocity structure and the reflectivity of the subsurface. VSP results are generally extrapolated from the vicinity of the borehole into the surrounding area to provide a 2-D velocity model. However, because of the heterogeneous nature of geothermal reservoirs, the error in extrapolating the VSP information can be minimized by conducting VSP surveys in multiple boreholes throughout the reservoir. The current study would have benefited from additional VSP data, which could have generated a more realistic velocity model. If it is determined that a surface seismic-reflection survey may provide more detailed information about the reservoir structure, we recommend adding geophones to any available borehole within the survey area. These datasets collected at depth provide an independent, low-cost alternative to the surface data and can help in the interpretation of the subsurface structure.

Seismic mapping is a robust method for converting travel-time differences to elevation changes, but it is an approximation that relies on a predefined reference velocity model. In the current study, the estimated elevation changes represent upper bounds of the actual changes, because the reference model is a 2-D velocity model that does not account for localized velocity heterogeneities. The results confirm the regional structure of the Basin and Range province. The general trend of the geologic units reveal a north-south strike and dip to the west, as expected for normal faulting encountered in the extensional regime on the western side of the Humbold Thrust Range. Furthermore, a local disturbance of this general pattern is detected by an elevation of the interface between the carbonate basement and the overlying sedimentary sequence. The structure, which resembles a horst, strikes east-west and appears to be extending throughout the survey area, cross-cutting the westward dipping units along the western boundary of the survey area. Previous studies corroborate the findings of the current

work, because the boundaries of the elevated structure co-locate with areas in which the first arrivals of seismic waves undergo a transition from strong to weak amplitudes (*Feighner et al.*, 1999). A possible explanation can be that of faults bounding the horst to the north and south. Such a fault is reported by *Teplow* (1999) based on 3-D seismic reflection data and is located along the southern flank of the elevated structure. Furthermore, gravity data reported in the same study indicates a residual gravity high that coincides with the areal extent of the horst in the central section of the Rye Patch reservoir. In addition tomography results (*Feighner et al.*, 1999) indicate an elevated high-velocity structure along the eastern border of the survey area. The synthesis of these results suggest the presence of a local structure resembling a horst, which can be modeled by an up-lift of the interface between the basement and overlying sediments. However, the data suggest that this up-lift does not extend to the surface, but comes to a halt between 50 m and 200 m depth.

The reported deviations are applicable to the interface between the basement and the overlying sediments. In general, the elevation changes can be projected onto the clastic reservoir at 880 m depth if strike, throw, and dip of the present faults are known. Because this information cannot be extracted from the current data, we did not attempt to map of the reservoir. However, most of the faults at Rye Patch reveal a steep dip angle and a vertical extension that exceeds the elevation difference between the basement interface (700 m) and the reservoir (880 m). Therefore, it can be assumed that the structure of the reservoir mimics that of the interface above.

One way to assess the validity of the presented model of the Rye Patch structure could be to incorporate and test it with current reservoir simulations. In general, however, it can be expected that the actual subsurface structure is a combination of the results derived from numerous studies at Rye Patch reservoir, and thus the combination of these surveys can be used as an example in exploring other geothermal reservoirs.

Acknowledgments. The authors would like to acknowledge reviews by Lane Johnson, Valeri Korneev, and Daniel Hawkes. This work was supported by the Assistant Secretary for Energy Efficiency and Renewable Energy, Office of Wind and Geothermal Technologies, of the US Department of Energy under Contract No. DE-AC03-76SF00098. Data processing was performed at the Center for Computational Seismology, which is supported by the Director, Office of Science, Office of Basic Energy Sciences, Division of Engineering and Geosciences, of the U.S. Department of Energy under Contract No. DE-AC03-76SF00098. The authors would like to thank Presco Energy LLC for the permission to use the data compiled in *Teplow* (1999). Most graphics were produced with the *Generic Mapping Tools* (Wessel and Smith, 1998).

References

Aki K., and Richards, P. G., 1980, Quantitative seismology, *Freemann*, New York, pp. 932.

Black, R. A., S. J. Deemer, and S. B. Smithson, 1991, Seismic reflection studies in Long Valley Caldera, California, *J. Geophys. Res.*, **96**, pp. 4,289-4,300.

Blackwell, D. D., 1985, A transient model of the geothermal system of the Long Valley Caldera, California, *J. Geophys. Res.*, **90**, pp. 11,229-11,242.

Dix, C. H., 1952, Seismic prospecting for oil, *Harper*, New York, pp. 414.

Feighner, M., Daley, T.M., Majer, E.L., 1998, Results of vertical seismic profiling at Well 46-28, Rye Patch geothermal field, Pershing County, Nevada, *Lawrence Berkeley National Laboratory Report LBNL-41800.*

Feighner, M., Gritto, R., Daley, T.M., Keers, H., Majer, E.L., 1999, Three-dimensional seismic imaging of the Rye Patch geothermal reservoir, *Lawrence Berkeley National Laboratory Report LBNL-44119.*

GeothermEx, 1997, Geology of the Rye Patch geothermal field, Pershing County, Nevada, *Internal Report, GeothermEx, Inc., Richmond, California.*

Hill, D. P., 1976, Structure of Long Valley caldera from seismic refraction experiments, *J. Geophys. Res.*, **81**, pp. 745-753.

Hill, D. P., Kissling, E., Luetgert J. H., and Kradolfer U., 1985, Constraints on the upper crustal structure of the Long Valley-Mono craters volcanic complex, Western California, from seismic refraction measurements, *J. Geophys. Res.*, **90**, pp. 11,135-11,150.

Nettleton, L. L., 1940, Geophysical prospecting for oil, *MacGraw-Hill Book Company*, New York, pp. 444.

Pakiser, L. C., Press, F., Kane, M. F., 1960, Geophysical investigations of Mono Basin, California, *Geol. Soc. Am. Bull.*, **71**, pp. 415-447.

SECO, 1998, 3-D seismic survey, Rye Patch geothermal field, Pershing County, Nevada, June-August 1998, *Report, Subsurface Exploration Company, Pasadena, CA.*

Sorey, M. L., 1985, Evolution and present state of the hydrothermal system in Long Valley Caldera, *J. Geophys. Res.*, **90**, pp. 11,219-11,228.

Telford, W. M., Geldard, L. P., and Sheriff, R. E., 1990, Applied geophysics, *Cambridge Univerity Press*, New York, pp. 770.

Teplow, B., 1999, Integrated geophysical exploration program at the Rye Patch geothermal field, Pershing County, Nevada - *Final Report*.

Wessel, P., and Smith, W. H. F., 1998, New, improved version of Generic Mapping Tools released, *EOS Trans. Amer. Geophys. U.*, **79**, No. 47. pp. 579.

* Corresponding Author: Roland Gritto, Earth Sciences Division, Lawrence Berkeley National Laboratory, 1 Cyclotron Road, MS 90-1116, Berkeley, CA 94720, phone: 510.486.7118, e-mail: rgritto@lbl.gov

[1]Center for Computational Seismology, Earth Sciences Division, Lawrence Berkeley National Laboratory, 1 Cyclotron Road, MS 90-1116, Berkeley, CA 94720, USA

Figure 1. Location map with area of 3-D seismic survey. The location of VSP Well 46-28 is indicated by the arrow.

Figure 2. Map indicating the locations of the source points (stars) during the 3-D seismic reflection survey and the location of wells 42-28, 44-28, 46-28, and 72-28 (circles). Axes of the current and following figures are given in plane state coordinates in feet.

Figure 3. Common receiver gather for a sources line north of well 46-28. The location of the receiver well is projected onto the data gather for reference.

Figure 4. Velocity profile from the VSP survey in well 46-28, with interpretation of geologic strada.

Figure 5. Velocity model and ray paths from source lines transecting well 46-28: **(a)** N-S direction; **(b)** E-W direction.

Figure 6. Schematic model of a low velocity layer over a high velocity basement with raypath from surface source to receiver in borehole.

Figure 7. Map of source locations of the 3-D seismic survey and locations of the migrated points where rays intersect the interface between carbonate basement and overlying sediments. The four boreholes are indicated by circles for reference (the well numbers have been omitted for graphic considerations).

Figure 8. Three-dimensional surface map of topography changes of the interface between carbonate basement and overlying sediments. The changes are mapped at each of the migrated points shown in Figure 7. The topography changes are relative to the interface at 700 m depth. The four boreholes are shown for reference. View from south-west. Vertical exaggeration of the current and all subsequent 3-D plots is about 5:1.

Figure 9. Three-dimensional map of the surface locations of the sources during the seismic-reflection survey. Elevation in meters above sea level. View from south-west.

Figure 10. Similar to Figure 8 with exception that sources are kept at the same elevation as well-head of borehole 46-28 during the ray tracing. View from south-west.

Figure 11. Contour map of the variations in elevation of the basement interface. Contour lines are in meters relative to the basement interface. The grey areas represent receiver locations where good first-arrival energy was recorded from far-offset shots during the 3-D seismic survey. The northern area recorded good first-arrival energy from shot number 2, located 7.4 km NW of the VSP well 46-28, while the southern area recorded good first arrival energy from shot number 4, located 5.2 km SSE of the VSP well. No strong first arrivals were recorded in the central region of the survey. The bold grey line represents the projection of a fault onto the basement interface that was interpreted by *Teplow* (1999) from 3-D seismic reflection data.

Figure 12. Seismic data recorded along a representative receiver line in the western part of the survey area. The source position was at shot number 2. Notice the abrupt change in amplitudes of the first arrivals, as indicated by the arrow.

Figure 13. Contour map of the Bouguer gravity residual in the central region of the 3-D seismic survey, as reported by *Teplow* (1999). The thick black line is superimposed for reference and represents the 0 m-contour line of the basement elevation as determined from the surface-to-borehole seismic data.

Figure 14. Velocity estimates of tomographic travel-time inversions for two receiver lines at the eastern boundary of the seismic survey area: **(a)** N-S receiver line, located above the maximum elevation of basement interface in Figure 8; **(b)** N-S receiver line, located directly east of the maximum elevation of basement interface in Figure 8.

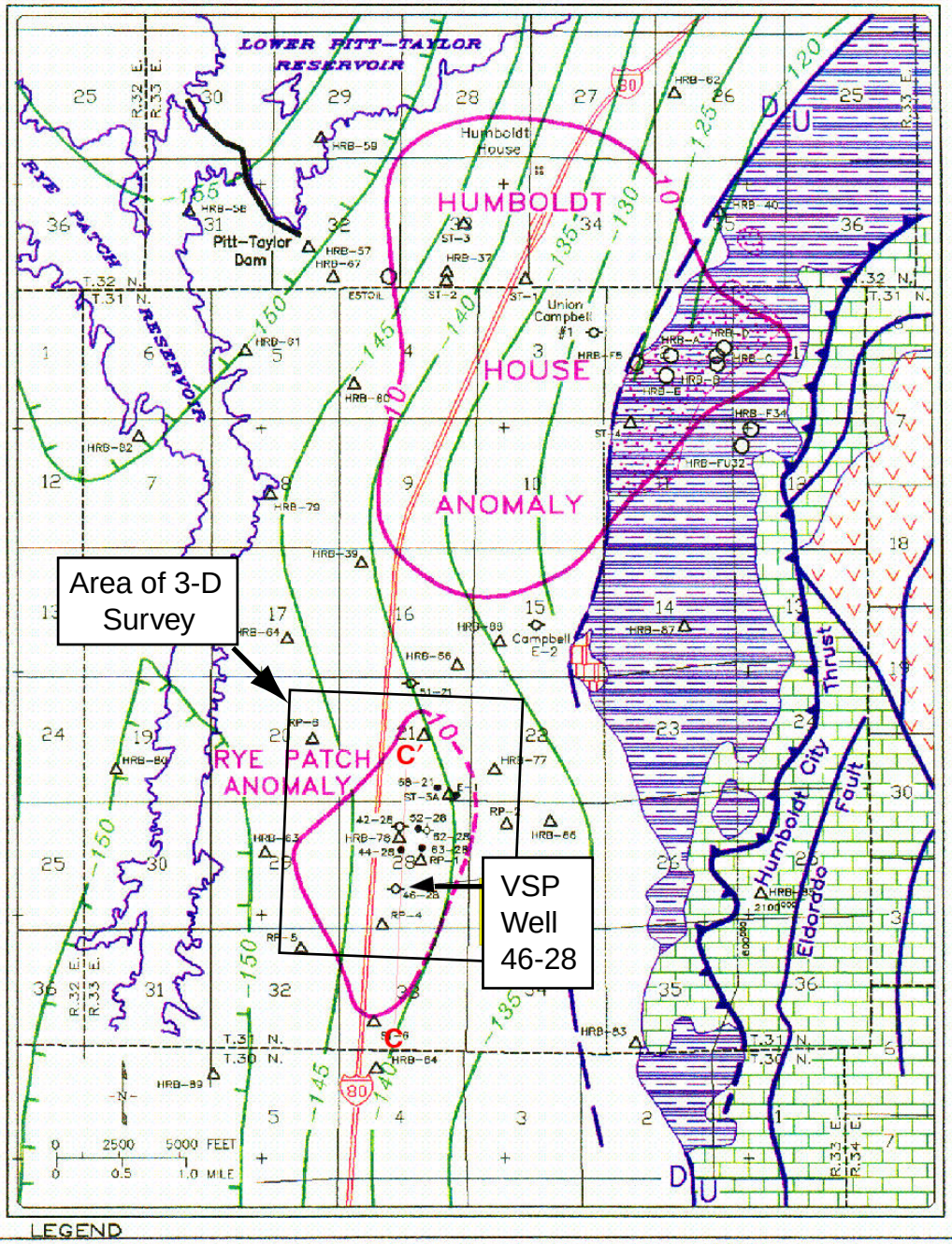
LOWER PITT-TAYLOR RESERVOIR
Pitt-Taylor Dam
RYE PATCH RESERVOIR
Humboldt House
HUMBOLDT HOUSE ANOMALY
RYE PATCH ANOMALY
Area of 3-D Survey
VSP Well 46-28
Union Campbell #1
Campbell E-2
Humboldt City Fault
Eldorado Thrust
T.32 N.
T.31 N.
T.30 N.
R.32 E.
R.33 E.
0 2500 5000 FEET
0 0.5 1.0 MILE
LEGEND
Line of equal complete bouguer gravity. Assumes a bedrock density of 2.67 g/cm3 (interval 5 mgals)
Shallow temperature gradient contour, °F/100'
Capable of production / dry hole
Strat test or gradient hole / mineral test hole
Plugged & abandoned well
Normal fault (dashed where inferred)
Thrust fault (teeth on upper plate)
Hydrothermally altered area
Quaternary alluvium or lake deposits
Tertiary basalt
Triassic Grass Valley Fm. (metamorphosed mudstone and sandstone)
Triassic Star Peak Group limestone (Natchez Pass and Pride Formations)
Triassic rhyolite porphyry and ash-flow tuff

Figure 1.

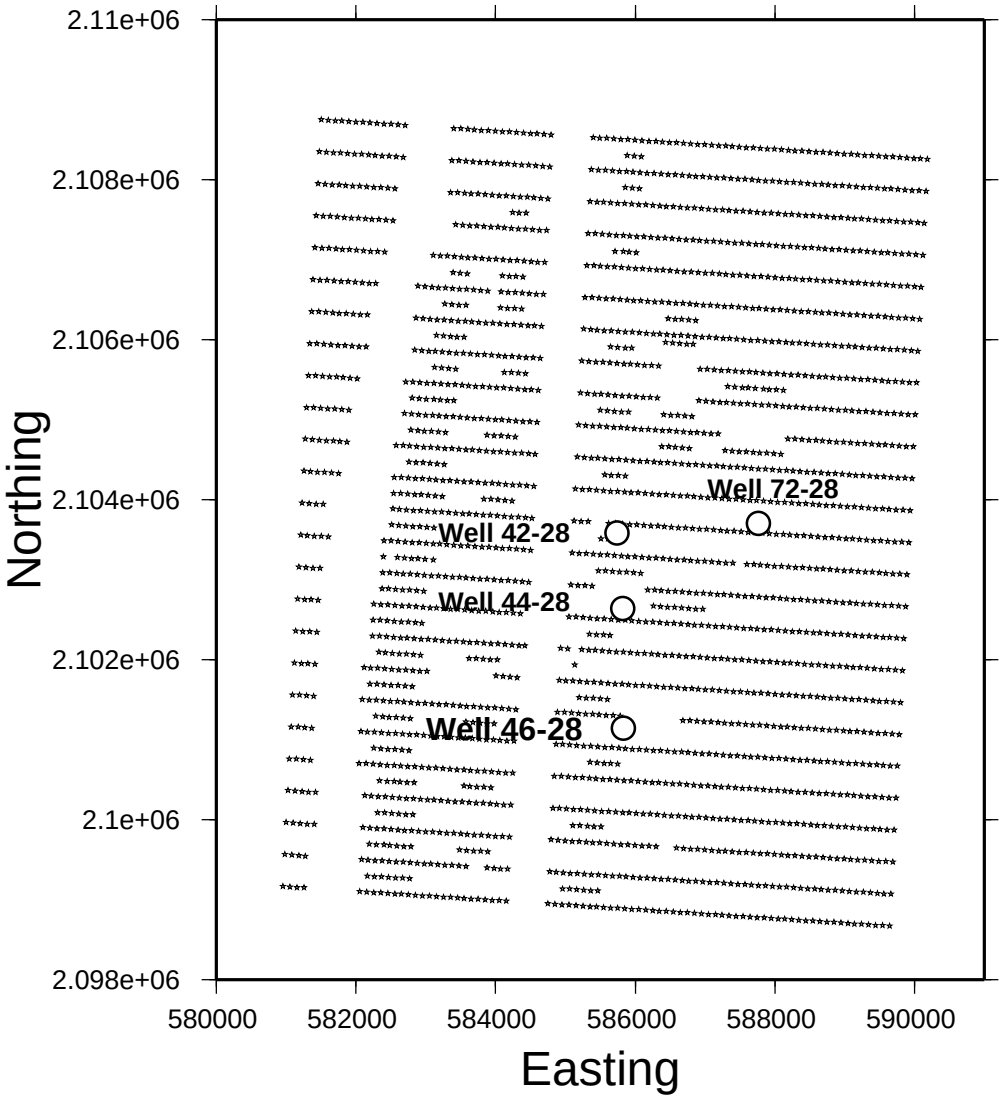
2.11e+06
2.108e+06
2.106e+06
2.104e+06
2.102e+06
2.1e+06
2.098e+06
Northing
580000
582000
584000
586000
588000
590000
Easting
Well 72-28
Well 42-28
Well 44-28
Well 46-28

Figure 2.

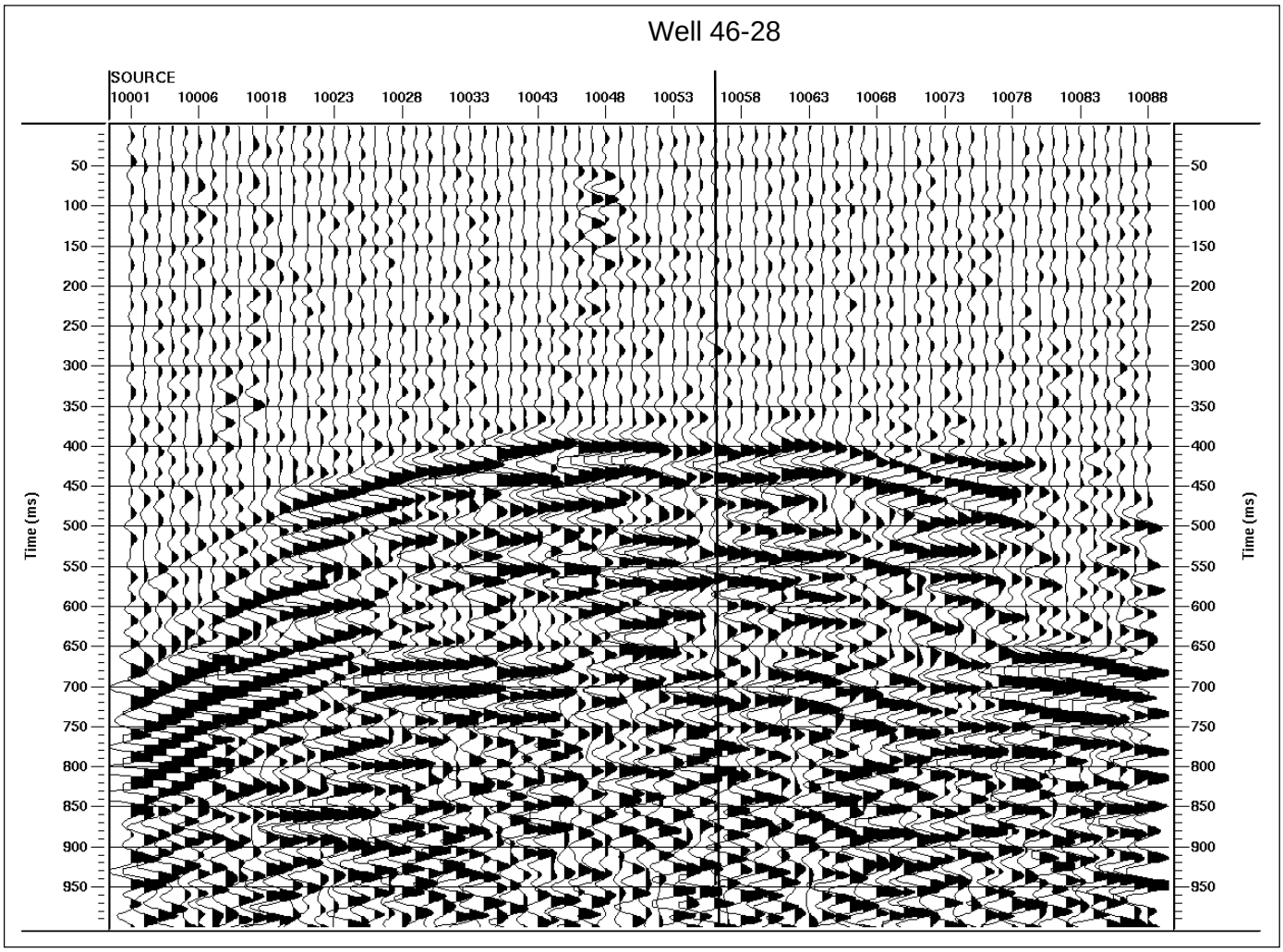
Well 46-28
SOURCE
10001
10006
10018
10023
10028
10033
10043
10048
10053
10058
10063
10068
10073
10078
10083
10088
Time (ms)
50
100
150
200
250
300
350
400
450
500
550
600
650
700
750
800
850
900
950

Figure 3.

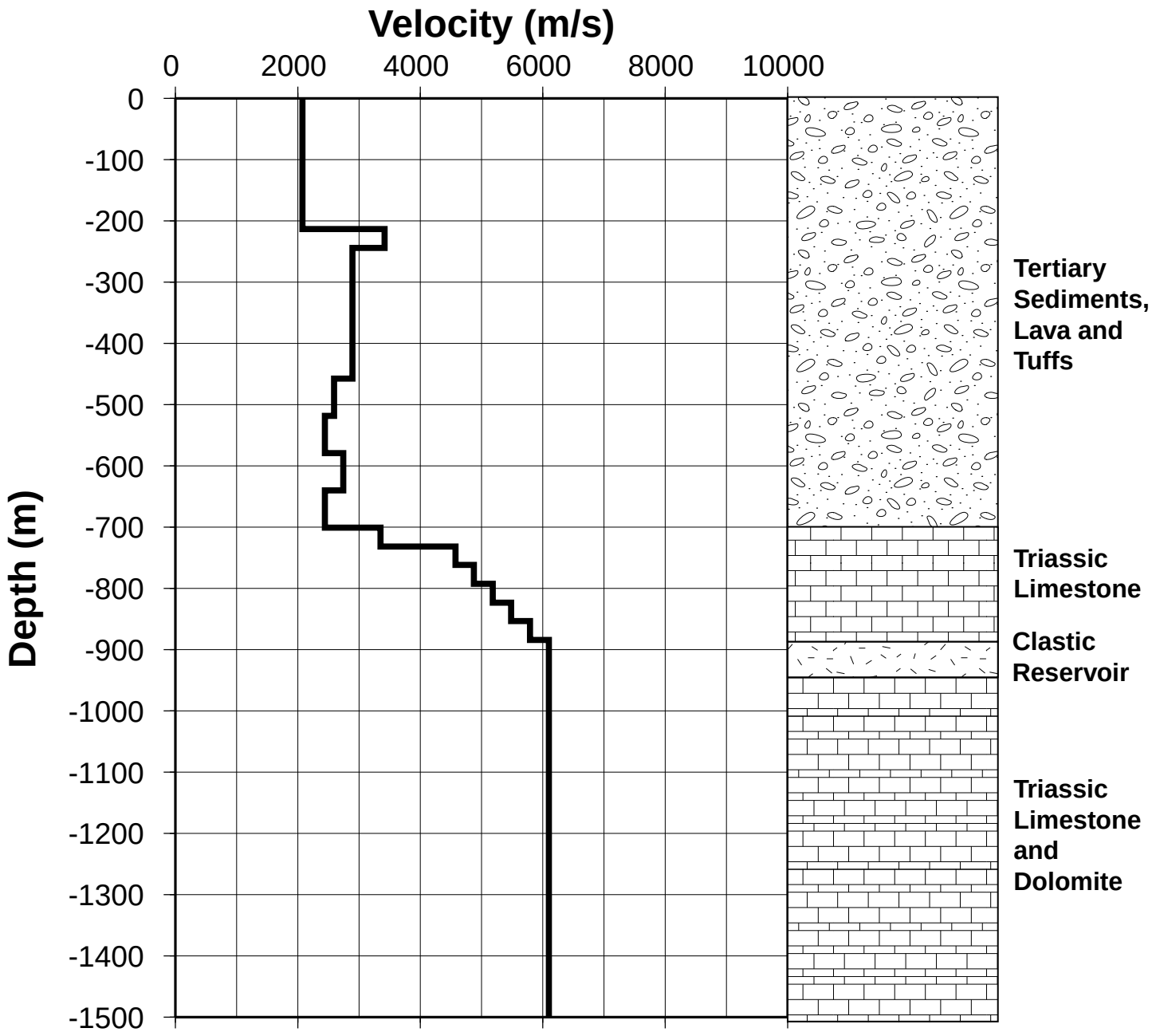
Velocity (m/s)
0
2000
4000
6000
8000
10000
Depth (m)
0
-100
-200
-300
-400
-500
-600
-700
-800
-900
-1000
-1100
-1200
-1300
-1400
-1500
Tertiary Sediments, Lava and Tuffs
Triassic Limestone
Clastic Reservoir
Triassic Limestone and Dolomite

Figure 4.

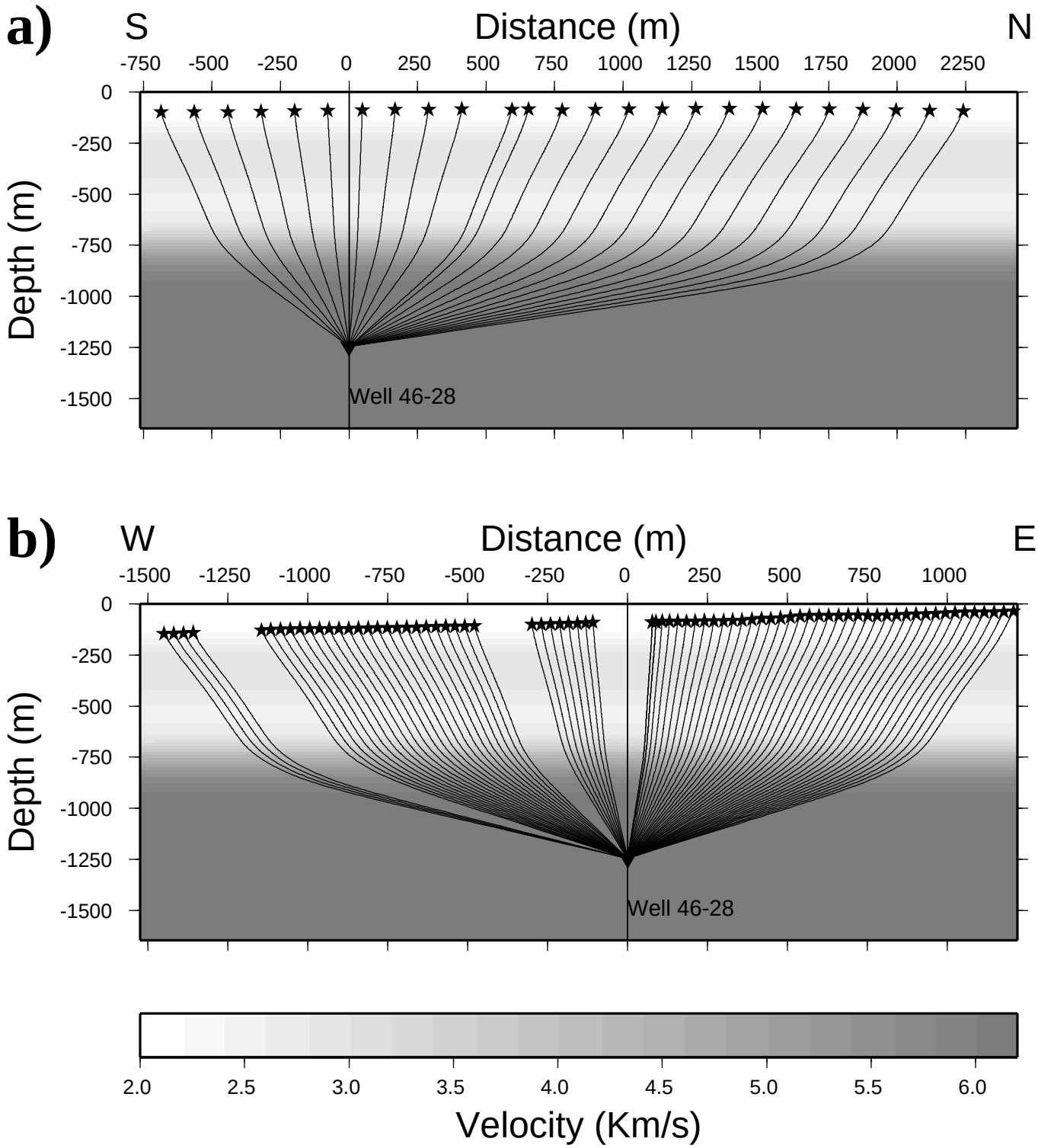
a)
S
Distance (m)
N
-750 -500 -250 0 250 500 750 1000 1250 1500 1750 2000 2250
0
-250
-500
-750
-1000
-1250
-1500
Depth (m)
Well 46-28
b)
W
Distance (m)
E
-1500 -1250 -1000 -750 -500 -250 0 250 500 750 1000
0
-250
-500
-750
-1000
-1250
-1500
Depth (m)
Well 46-28
2.0 2.5 3.0 3.5 4.0 4.5 5.0 5.5 6.0
Velocity (Km/s)

Figure 5.

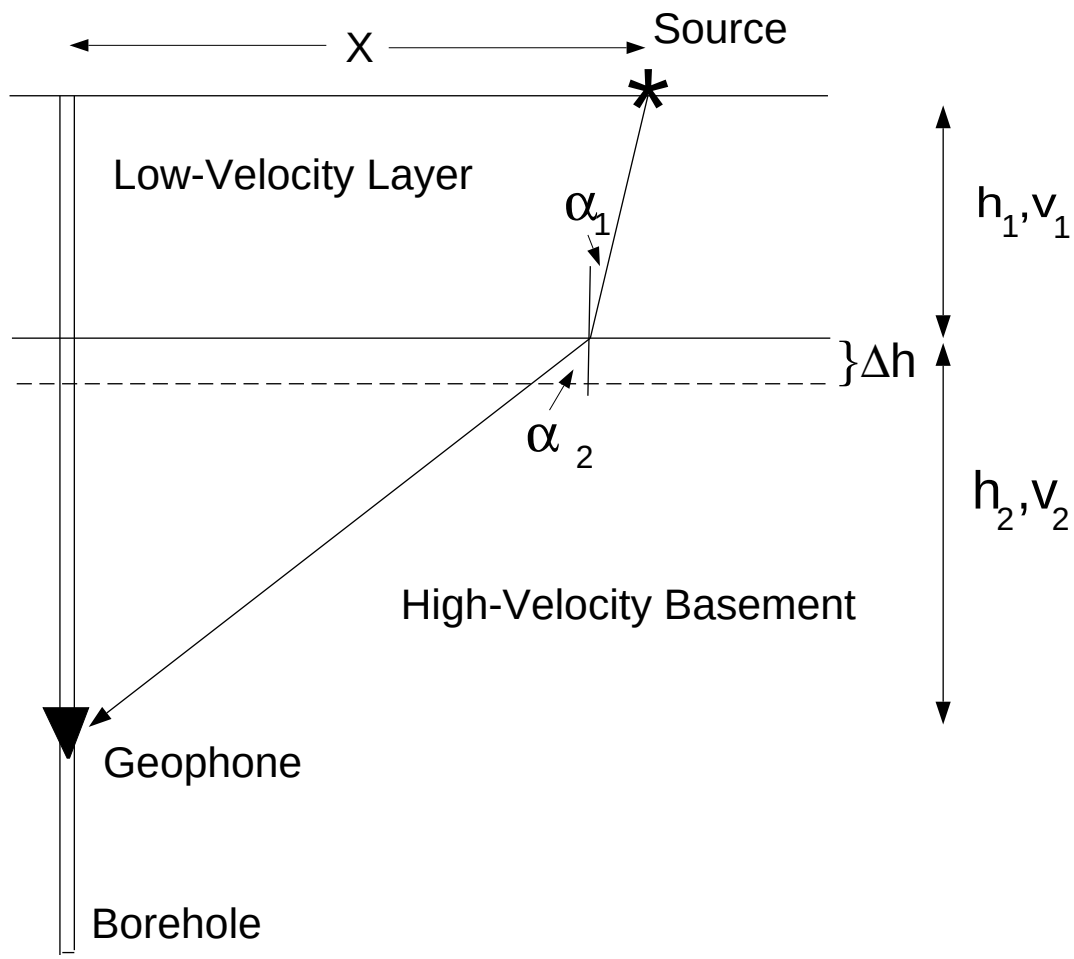
X
Source
Low-Velocity Layer
α1
h1,v1
}Δh
α 2
h2,v2
High-Velocity Basement
Geophone
Borehole

Figure 6.

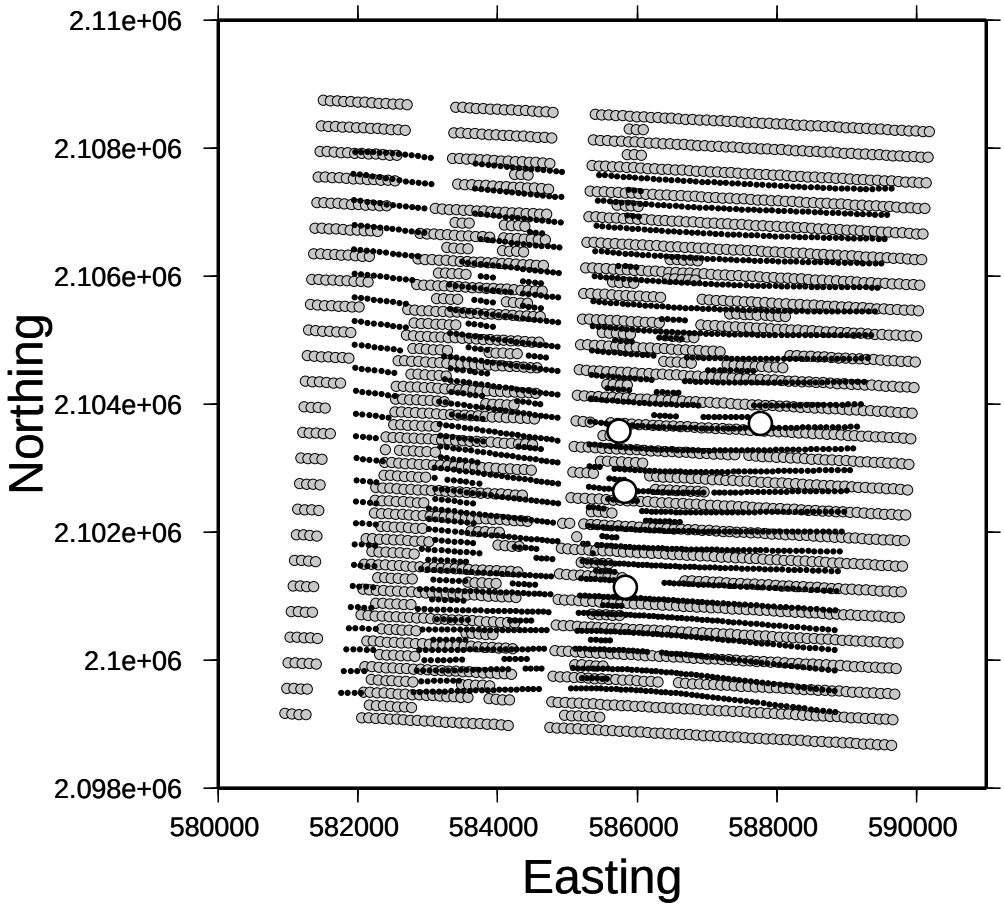
2.11e+06
2.108e+06
2.106e+06
2.104e+06
2.102e+06
2.1e+06
2.098e+06
Northing
580000
582000
584000
586000
588000
590000
Easting

Figure 7.

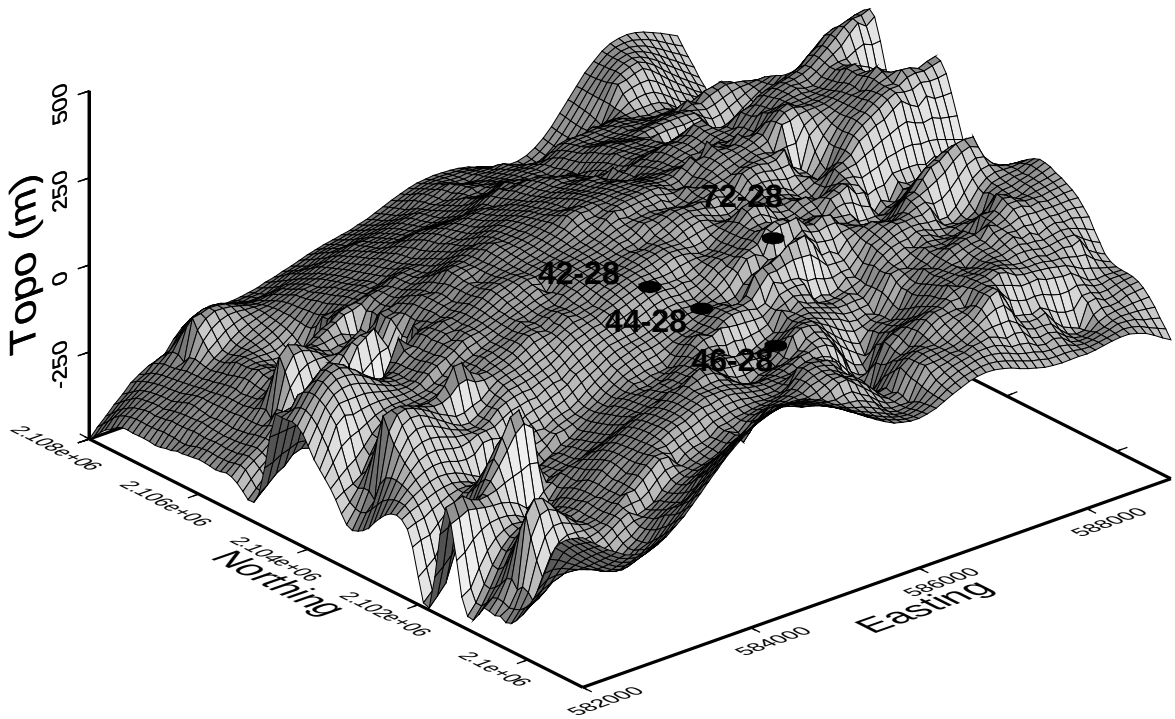
Topo (m)
500
250
0
-250
72-28
42-28
44-28
46-28
2.108e+06
2.106e+06
2.104e+06
2.102e+06
2.1e+06
Northing
582000
584000
586000
588000
Easting

Figure 8.

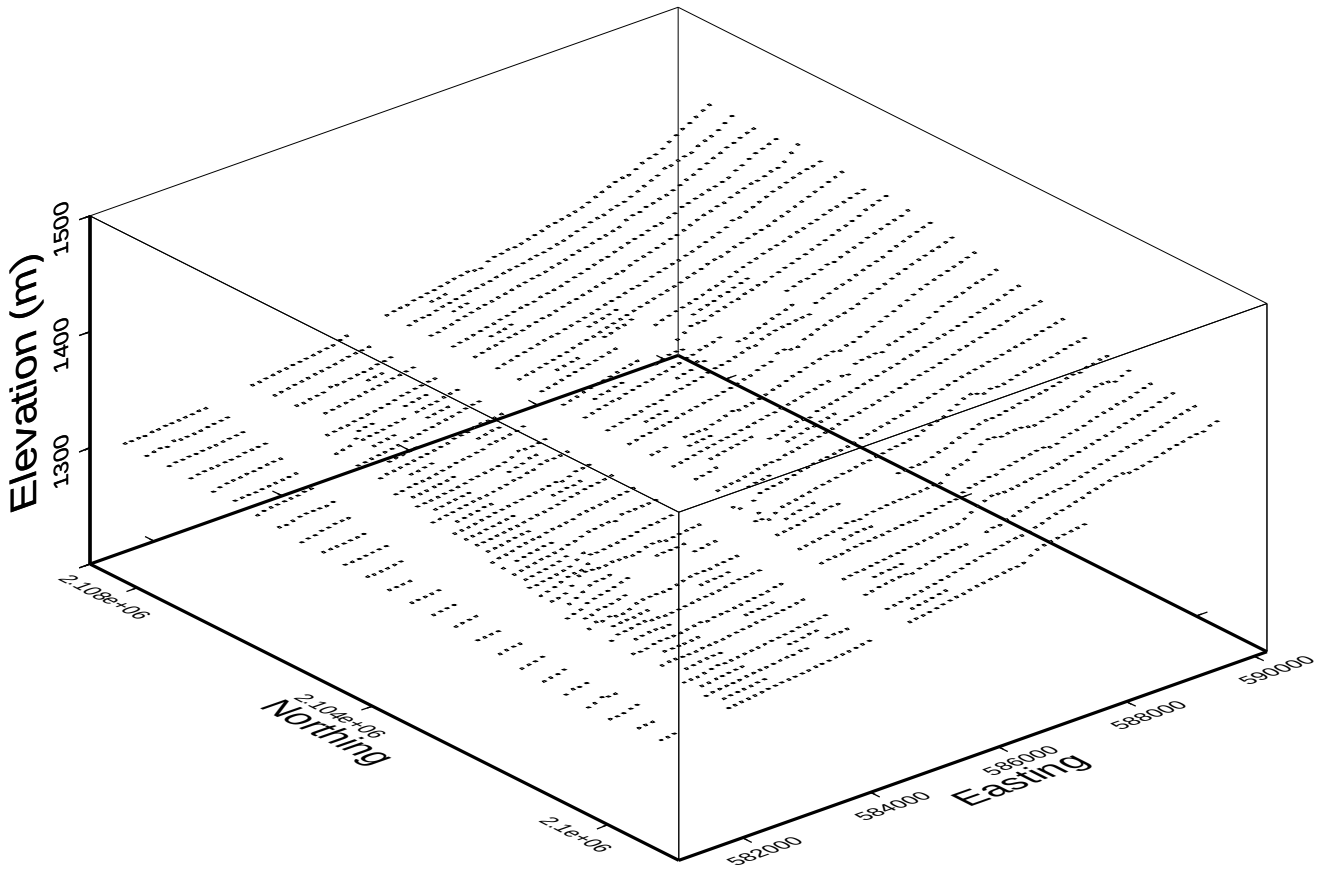
Elevation (m)
1300
1400
1500
Northing
2.108e+06
2.104e+06
2.1e+06
Easting
582000
584000
586000
588000
590000

Figure 9.

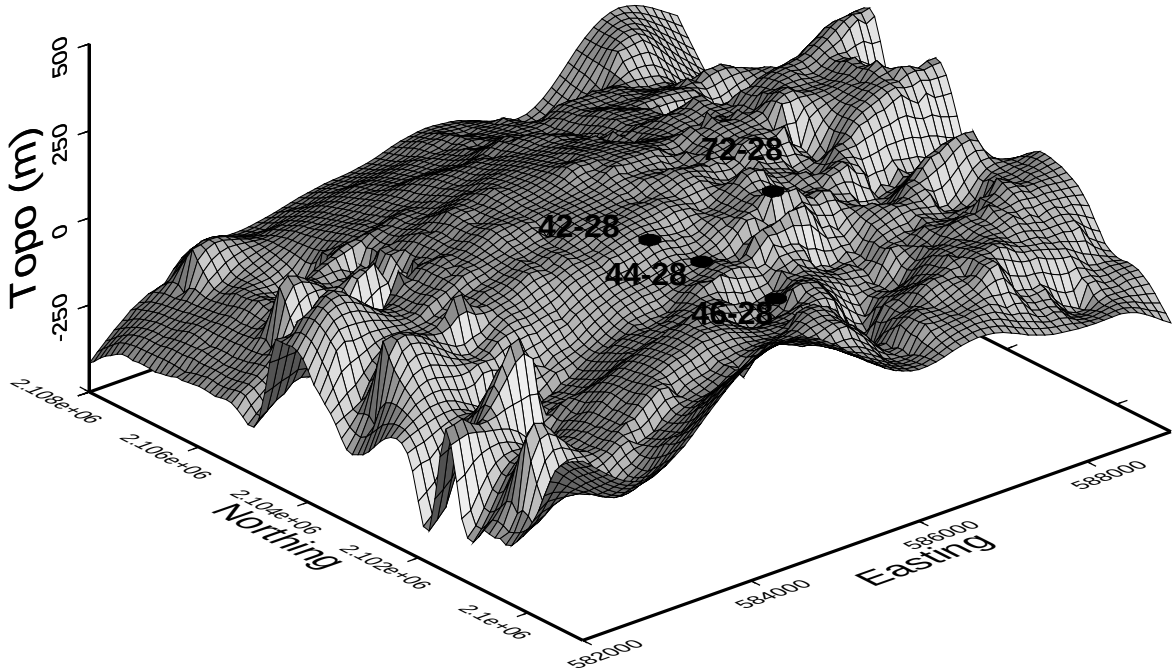
Topo (m)
500
250
0
-250
72-28
42-28
44-28
46-28
2.108e+06
2.106e+06
2.104e+06
2.102e+06
2.1e+06
Northing
582000
584000
586000
588000
Easting

Figure 10.

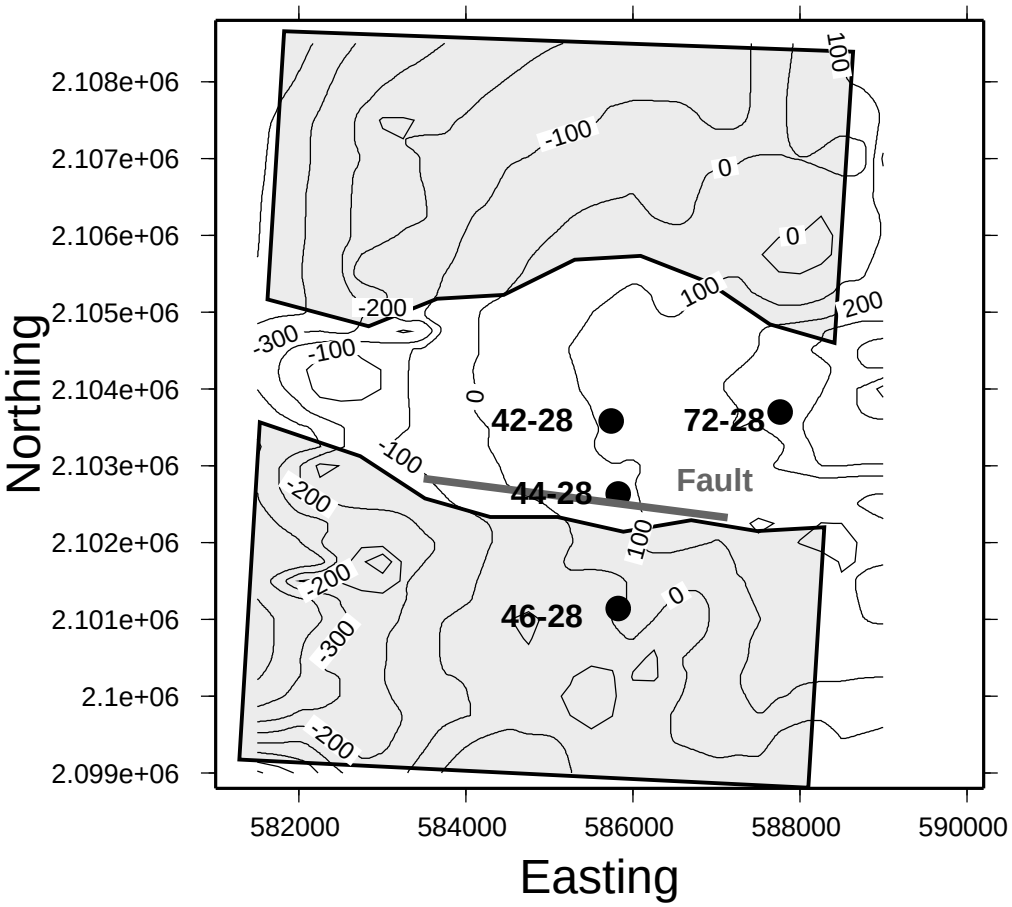
2.108e+06
2.107e+06
2.106e+06
2.105e+06
2.104e+06
2.103e+06
2.102e+06
2.101e+06
2.1e+06
2.099e+06
Northing
582000
584000
586000
588000
590000
Easting
42-28
72-28
44-28
46-28
Fault
100
-100
0
0
-200
100
200
-300
-100
0
-100
-200
100
-200
0
-300
-200

Figure 11.

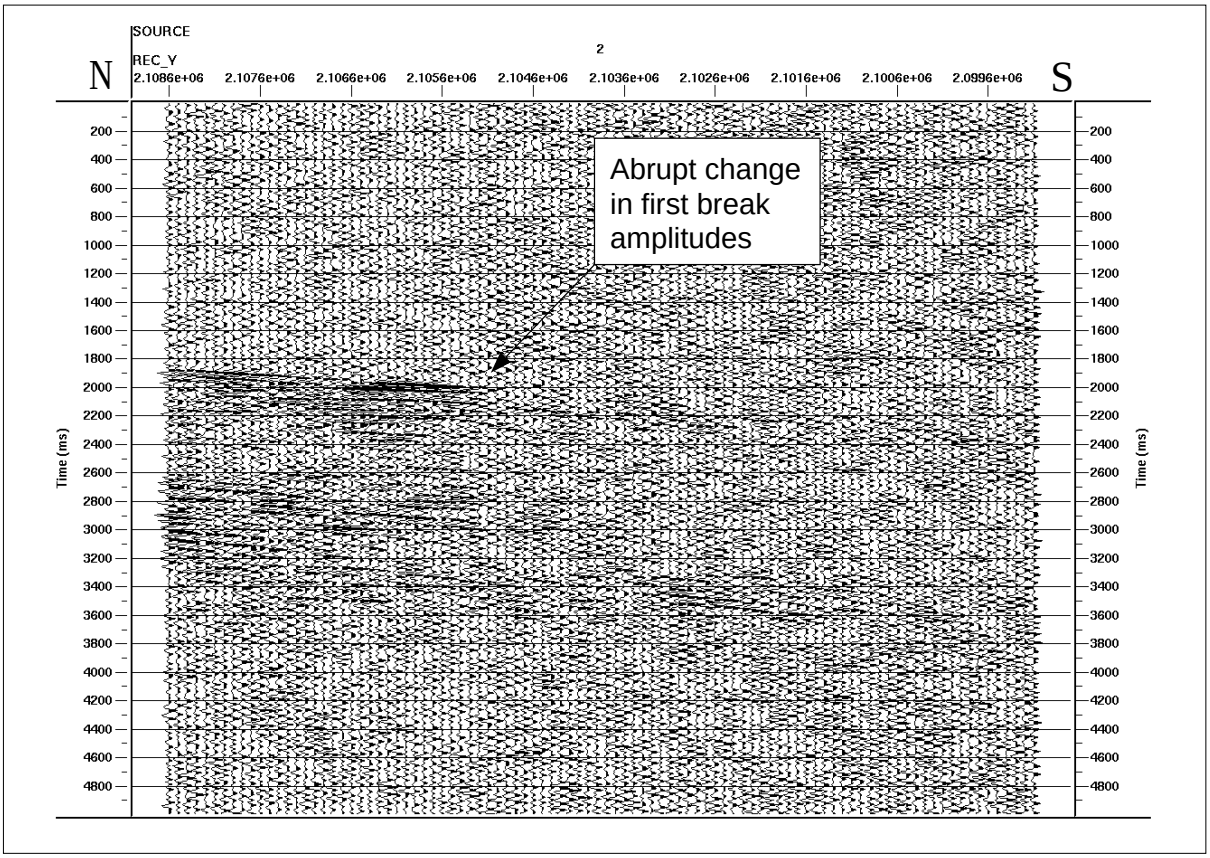
SOURCE
REC_Y
2
N
S
2.1086e+06
2.1076e+06
2.1066e+06
2.1056e+06
2.1046e+06
2.1036e+06
2.1026e+06
2.1016e+06
2.1006e+06
2.0996e+06
Time (ms)
200
400
600
800
1000
1200
1400
1600
1800
2000
2200
2400
2600
2800
3000
3200
3400
3600
3800
4000
4200
4400
4600
4800
Abrupt change in first break amplitudes

Figure 12.

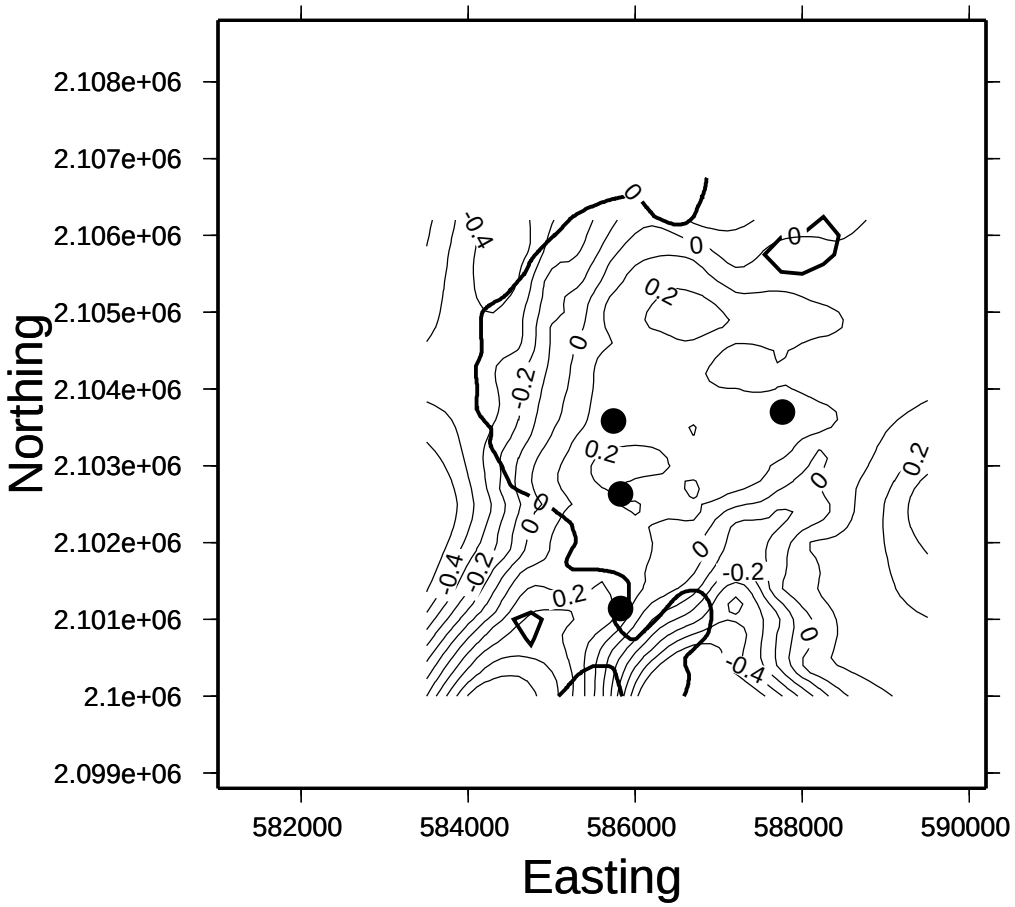
2.108e+06
2.107e+06
2.106e+06
2.105e+06
2.104e+06
2.103e+06
2.102e+06
2.101e+06
2.1e+06
2.099e+06
Northing
582000
584000
586000
588000
590000
Easting
0
0.2
-0.2
-0.4

Figure 13.

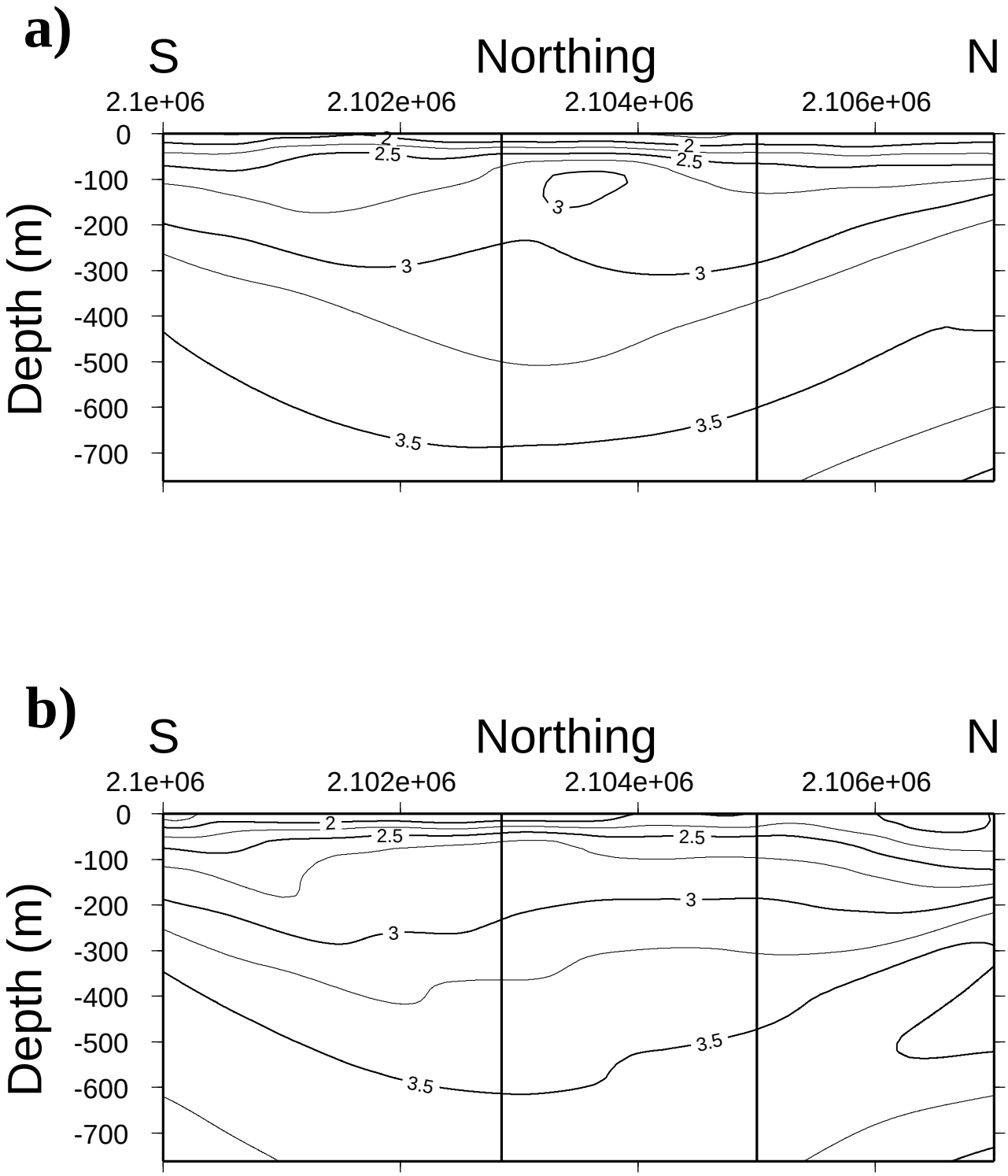
a)
S
Northing
N
2.1e+06
2.102e+06
2.104e+06
2.106e+06
Depth (m)
0
-100
-200
-300
-400
-500
-600
-700
2
2.5
3
3.5
b)
S
Northing
N
2.1e+06
2.102e+06
2.104e+06
2.106e+06
Depth (m)
0
-100
-200
-300
-400
-500
-600
-700
2
2.5
3
3.5

Figure 14.